ADVANCED ELECTRONIC MATERIALS Open Access
www.advelectronicmat.de

Solvated PbI_2 Clusters Preceding the Crystallization of Lead Halide Perovskites–a UV/VIS In Situ Study

*Maximilian Spies, Simon Biberger, Fabian Eller, Eva M. Herzig, and Anna Köhler**

The solution-based fabrication of reproducible, high-quality lead iodide perovskite films demands a detailed understanding of the crystallization dynamics, which is mainly determined by the perovskite precursor solution and its processing conditions. A systematic in situ study is conducted during the critical phase before the nucleation in solution to elucidate the formation dynamics of lead iodide perovskite films. Using ultraviolet (UV) absorption spectroscopy during spin coating allows to track the evolution of iodoplumbate complexes present in the precursor solution. It is found that prior to film formation, a novel absorption signature at 3.15 eV arises. This is attributed to the emergence of a PbI_2-DMF solvated (PDS) phase. The amount of PDS phase is closely connected to the concentration of the solution layer during spin coating. It is also proposed that PDS clusters are a predecessor of crystalline perovskite phases and act as nucleation seeds in the precursor solution. In this way, this work provides insights into the early stages of perovskite crystallization.

1. Introduction

The use of hybrid metal halide perovskites in solar cells has led to remarkable photovoltaic performances in the recent years. Devices with a single active perovskite layer (27.0% power conversion efficiency), as well as tandem devices with silicon and perovskite working in conjunction (34.6%) have demonstrated the potential for photovoltaic applications.[1] In addition, in a solution-based approach, low-cost processing techniques make perovskite film fabrication very affordable. For this, the perovskite precursors are often dissolved in a polar aprotic solvent. However, further processing such as spin coating or blade coating of the solution poses challenges in obtaining a suitable layer of polycrystalline perovskite on the substrate.[2,3] The resulting film should be fully covering, pin-hole free and consist of large crystal grains with only few defects.[2] Therefore, understanding the mechanisms during processing that dictate the crystallization in the precursor solution is important for the reproducible fabrication of neat perovskite films.

The properties of perovskite precursor solutions have already been extensively investigated. For instance, the optical properties of the precursor solution of methylammonium lead iodide ($MAPbI_3$), i.e., a solution made with the educts methylammonium iodide (MAI) and lead iodide (PbI_2), are known to result from iodoplumbate complexes.[4,5] In fact, iodine as well as solvent molecules is able to coordinate to the lead atom and the metal-to-halide charge transfer determines the absorption properties of these complexes.[5] Therefore, an absorption peak can be assigned to each lead complex with a specific iodine coordination (i.e., PbI^+, PbI_2, PbI_3^-, PbI_4^{2-}, ...).[5,6] The energetic positions of these highly absorbing species are located in the ultraviolet (UV) region and are not affected by the solvent.[5–7] However, solvent molecules compete with iodine for coordination sites to the lead.[7] Consequently, solvents with greater coordinating abilities result in an iodoplumbate complex distribution favoring complexes with lower iodine coordination.[7] Another property of the lead iodide perovskite precursor solution is its colloidal nature with size distributions in the range of 100–1 000 nm, measured using dynamic light scattering, as well as in the range of 1–10 nm obtained from small angle neutron scattering and cryo-electron microscopy.[8–11] The nanometer sized colloids outweigh the larger colloids substantially.[10] Despite these extensive investigations, the process of precursor formation and subsequent perovskite crystallization is still not fully understood.

In this work, we optically investigate the precursor solution of lead iodide perovskites with dimethylformamide (DMF) and dimethyl sulfoxide (DMSO) as solvents. The two solvents differ in their ability to coordinate with the iodoplumbate complexes, with DMSO being the more strongly coordinating solvent. We focus on the dynamic process of film formation. For both, as-prepared solutions and during spin coating (in situ), we obtain UV absorption data at concentrations suitable for thin film fabrication

M. Spies, S. Biberger, A. Köhler
Soft Matter Optoelectronics (EP II)
University of Bayreuth
95440 Bayreuth, Germany
E-mail: anna.koehler@uni-bayreuth.de
F. Eller, E. M. Herzig
Dynamics and Structure Formation – Herzig Group
University of Bayreuth
95440 Bayreuth, Germany

The ORCID identification number(s) for the author(s) of this article can be found under https://doi.org/10.1002/aelm.202500060

DOI: 10.1002/aelm.202500060

(0.2–0.9 mol L^{-1}). For all investigated solutions, we observe the emergence of a novel optical signature during spin coating. We ascribe this signature to a PbI_2-DMF solvated (PDS) phase. We propose that PDS clusters form in the precursor solution and act as nucleation seeds for the crystallization of subsequent perovskite phases. By modeling the solution layer thickness during spin coating, we estimate the precursor concentration in solution and find that the in situ observed optical evolution of the perovskite precursor solution is mainly concentration driven.

2. Experimental Section

2.1. Preparation of Solutions

All materials were used as received. Lead(II) iodide (PbI_2, 98%), methylammonium iodide (MAI, 99%), and formamidinium iodide (FAI, 99%) were purchased from TCI. The solvents dimethylformamide (DMF) and dimethyl sulfoxide (DMSO) were purchased from Acros. For $MAPbI_3$ (/$FAPbI_3$) solutions, PbI_2 and MAI (/FAI) were weighed in a stoichiometry of 1:1 and dissolved in DMF or in a solvent mixture DMF:DMSO = 12:1 at various concentrations (0.2–0.9 mol L^{-1}). For PbI_2 solutions, PbI_2 was dissolved in DMF at a concentration of 0.3 mol L^{-1}, making it comparable with the 0.6 mol L^{-1} $MAPbI_3$ (/$FAPbI_3$) precursor solutions.

2.2. As-Prepared Measurements

The as-prepared measurements were conducted with the Thinning Fluid Film Spectroscopy (TFFS) method recently introduced by Eller et al.[12] In this method, quartz tubes, partially filled with solution and sealed in inert N_2 atmosphere, are rapidly shaken with a home-built robotic setup. Transmission is measured through the thin fluid film on the walls of the tubes. This solution layer is thinning with time as it is flowing down the walls. Below a certain thickness, the absorption of the liquid layer is within the detection limits of the setup and can hence be measured. This procedure yields the spectral shape of the absorption, albeit the extinction cannot be determined quantitatively as the thickness of the solution layer on the wall of the tube is not known. The light source was a deuterium lamp from Ocean Optics and the spectrometer an AvaSpec-HSC1024×58 TEC-EVO from Avantes.

2.3. In Situ Measurements

All optical in situ data were recorded with a home-built setup. A detailed description of this setup was provided by Buchhorn et al.[13] In brief, solutions were spin coated on a quartz glass substrate at 2 000 rpm for 60 s and a ramp-up time of 1 s, and the transmitted light was recorded at a frame rate of 7 Hz. A halogen lamp in combination with a deuterium lamp was used as light source. To ensure reproducibility, at least two coatings were recorded for each sample, which turned out to be quasi-identical.

3. Results

3.1. Unraveling Spectral Signatures in Concentrated Precursor Solution

We first focus on identifying the various spectral signatures in concentrated precursor solutions. Absorption spectra of a perovskite precursor solution at concentrations suitable for film fabrication (≈1 mol L^{-1}) are generally difficult to obtain due to the strongly absorbing properties of the iodoplumbate complexes. In previous studies, absorption spectra were obtained only by diluting the precursor solution to the mmol L^{-1} range.[5,6,14] However, since the colloidal nature of the precursor solution is strongly concentration dependent, the properties of dilute solutions may not necessarily be identical to solutions with higher concentrations.[8] It is therefore essential to investigate the precursor solution at concentrations that are relevant for the fabrication of perovskite-based optoelectronic devices.

We measured the absorption of precursor solutions up to a concentration of 0.9 mol L^{-1}, using the TFFS method described above.[12] We employed a sealed quartz glass tube containing solution and nitrogen gas to avoid solvent evaporation and exposure to oxygen or water. In contrast to the in situ method described later in this work, we refer to measurements of the perovskite precursor solution in the TFFS setup as as-prepared. **Figure 1** shows the spectra obtained by absorption measurements of stochiometric $MAPbI_3$ as-prepared precursor solutions made with pure dimethylformamide (DMF) in Figure 1a. The absorption spectra of precursor solutions made with DMF and dimethyl sulfoxide (DMSO) (DMF:DMSO = 12:1) as solvents are displayed in Figure 1b. The spectra are normalized to the area under the curve from 2.7 to 3.7 eV (At energies above 3.7 eV, there is an increased risk of artefacts from scattering, vide infra).

For the 0.2 mol L^{-1} DMF solution (Figure 1a), we observe three peaks at 2.90, 3.36, and 3.86 eV superimposed on a general increase of the absorption toward even higher energies. Other groups that investigated solutions in the mmol L^{-1} range observed the same features and attributed them to absorption from PbI_4^{2-}, PbI_3^{-}, and PbI_2 complexes, respectively.[5,6,14] Upon increasing the concentration up to 0.9 mol L^{-1}, we find the peaks associated with PbI_2 and PbI_4^{2-} to reduce in intensity relative to the feature attributed to PbI_3^{-}. Moreover, an isosbestic point is clearly visible at 3.32 eV.

In solutions containing a mixture of DMF and DMSO (Figure 1b), we observe a similar evolution, with an isosbestic point at 3.37 eV. Furthermore, we find a more pronounced PbI_2 signature compared to PbI_3^{-} and PbI_4^{2-}, especially at the lower concentration of 0.2 mol L^{-1}. We attribute this to the higher Gutmann Donor Number of DMSO (D_N = 29.8) compared to DMF (D_N = 26.6).[7] The Gutmann Donor Number is a measure for the coordination ability of a solvent. Since the iodine competes with the solvent for coordination sites to the lead, a more strongly coordinating solvent shifts the distribution of iodoplumbate complexes toward those with fewer iodine atoms. This effect is more pronounced in solutions with lower concentrations as they contain a higher ratio of solvent to iodine.

The concentration range in Figure 1 allows for a first tentative assignment of the spectral features. However, when preparing a perovskite film by spin-coating a precursor solution, the

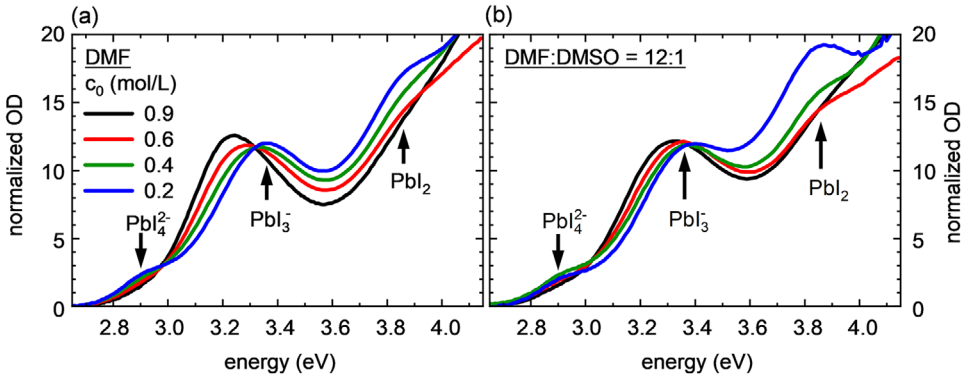

Figure 1. Absorption measurements of the as-prepared precursor solution of $MAPbI_3$ at various concentrations c_0, normalized by area up to 3.7 eV. a) the solvent in use is pure DMF, b) a small amount (1:12 by volume) of DMSO is added to DMF. Arrows indicate literature values for energies of the complexes PbI_2, PbI_3^-, and PbI_4^{2-}.

precursor concentration increases even further during processing and the film eventually crystallizes. The changes in absorption during one-step spin coating (in situ) of $MAPbI_3$ precursor solutions are captured in **Figure 2**.

Figure 2a depicts an in situ measurement during spin coating of stochiometric $MAPbI_3$ precursor in DMF at a concentration of 0.6 mol L^{-1} (see Figure S1, Supporting Information for 0.4 and 0.2 mol L^{-1}). We observe an evolution of the absorption at energies usually associated with the PbI_3 peak, i.e., in the spectral range of 3.0–3.5 eV. "Spinning time = 0 s" marks the beginning of spin coating. In the first few seconds, the spectra cannot be fully resolved as the absorption of the solution layer is still too high. After ≈2 s, the optical density (OD) decreases due to material throw-off, so that absorption spectra suitable for analysis can be recorded. At this point, the spectra obtained in general, and in particular the PbI_3^- peak positions, are in good agreement with the peak positions of the as-prepared solution measurements. Up to 5 s the OD decreases whereas, from 6 s onward, the OD maximum increases until it saturates the detector after 14 s. We ascribe the broad increase of the OD after 14 s to the formation of the highly scattering and absorbing intermediate phase $(MA)_2Pb_3I_8(DMF)_2$.[15,16]

Within the time between 2–14 s, we observe a narrowing of the band initially between 3.0–3.5 eV and a continuous shift of the band maximum (at 3.27 eV at 2 s) to the red (to 3.15 eV) until spectra can no longer be recorded. Additionally, we note an isosbestic point at 3.32 eV between 7–12 s, displayed in the bottom panel of Figure 2a as zoom-in. This isosbestic point occurs in the film formation at a stage where material throw-off no longer contributes to spectral changes. Hence, it suggests that the observed optical signatures do not originate from a single PbI_3^- peak but rather from two peaks with different widths and energetic positions and with varying intensity. Therefore, we conjecture that the spectral band in the range from 3.0 to 3.6 eV in the beginning (2–5 s) contains a significant contribution from the well-known PbI_3^- peak, whereas in the end (6–13 s) the emergence of a novel optical signature with its maximum at 3.15 eV modifies the absorption spectra.

To explain the spectral evolution over the range of 2.6 to 4.0 eV, we explore whether the spectra can be reproduced by assuming a superposition of absorption from the iodoplumbate complexes PbI_4^{2-}, PbI_3^-, and PbI_2. Therefore, we employed a model of three gaussian line shapes with fixed widths and at fixed positions, chosen at the literature energies of PbI_4^{2-}, PbI_3^-, and PbI_2, in agreement with the peaks in the low-concentrated as-prepared measurements.[5,6,14] Fitting the spectrum of the as-prepared precursor solution results in a discernible residual, which is depicted by the orange hatched area in Figure 2c. The residual consists of a nearly Gaussian peak centered at 3.18–3.15 eV and a general increase above 3.6 eV. We attribute the residual to an absorption band of a novel species.

We next studied the spectral composition of precursor solution during spin coating. To avoid artifacts from interferences below 2.8 eV and from scattering above 3.7 eV, we chose to keep the relative heights (and hence the areas) of the Gaussians associated with the iodoplumbate complexes fixed to the values obtained in the as-prepared solution. We find that the novel optical signature increases with spinning time relative to the iodoplumbate contributions (see Figure 2b). Additionally, the energetic position of the near Gaussian part slightly shifts from 3.18 to 3.15 eV with time. When we allow the heights of all Gaussians to vary, we still obtain essentially the same result, i.e., the new optical signature increases and red-shifts with spinning time, and the heights of the Gaussian peaks associated with the iodoplumbate complexes increase from PbI_4^{2-} to PbI_2 (see Figure S2, Supporting Information). To keep the number of fitting parameters low, we hence kept the relative heights of the iodoplumbate Gaussians fixed for all further analysis. Fits to spectra at other initial concentrations (0.2–0.9 mol L^{-1}) show qualitatively similar evolutions, albeit the magnitude of the novel optical signature increases with initial concentration (Figure 2c). The fits to in situ measurements with different initial concentrations are displayed in Figure S3 and the supporting video files (Supporting Information).

Hence, the data so far support the notion of a novel species forming in proportion to the precursor concentration, be it the initial concentration or the increase in concentration during spin coating. The evolution of the spectra with increasing concentration, notably the shift of the band centered around 3.2 eV, its narrowing and the emergence of an isosbestic point are difficult to account for without postulating an additional species. We can rule out a sole solvatochromic effect as explanation for the observed shift, since this cannot account for the isosbestic point

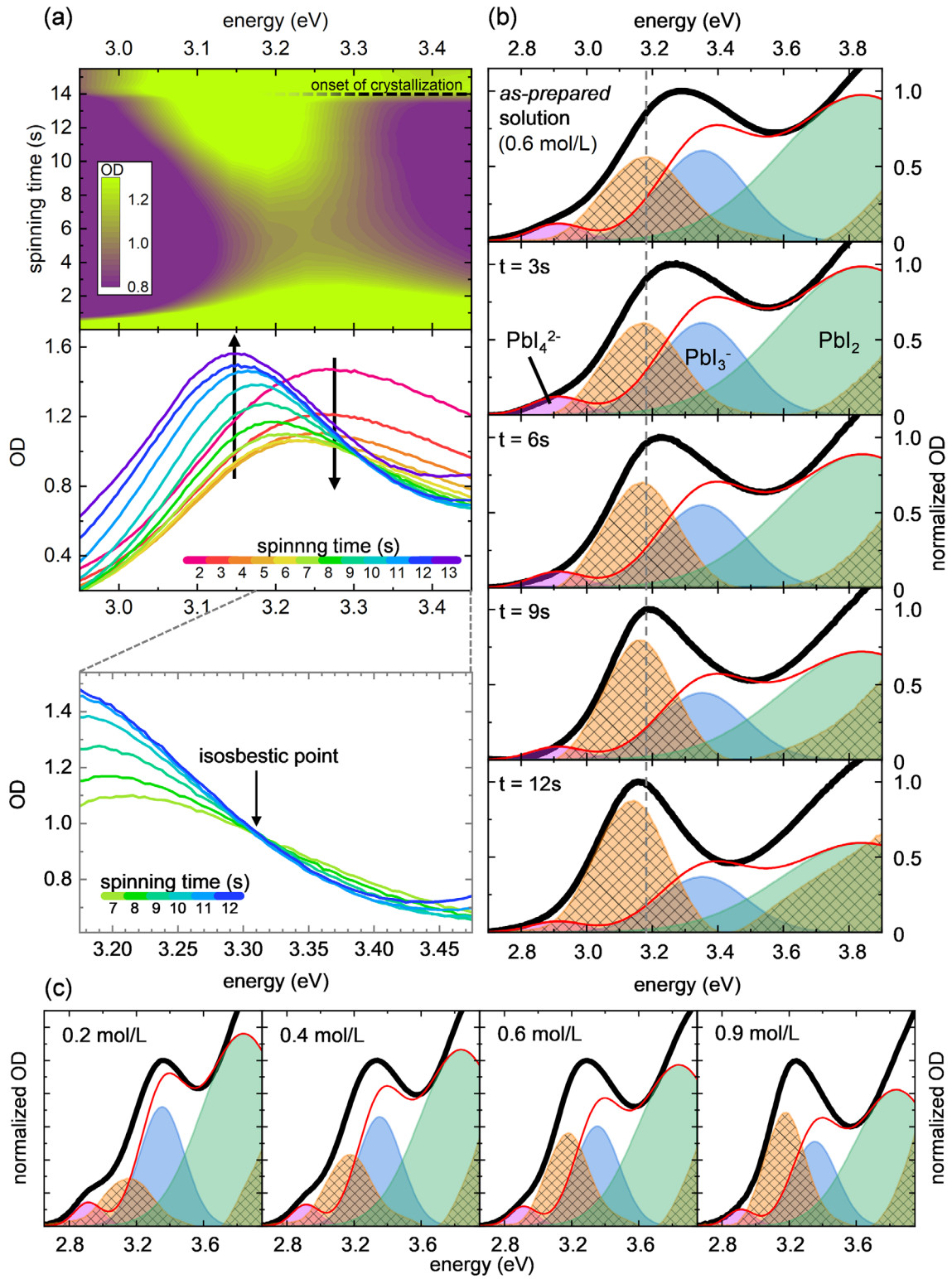

Figure 2. a,b) In situ absorption measurements of the $MAPbI_3$ precursor solution in DMF at 0.6 mol L^{-1} during spin coating, highlighting the evolution of the central peak around 3.2 eV. a) 2D map of the OD with respect to energy and spinning time (top), temporal cuts through the OD map (middle) and zoom to an isosbestic point after 6 s (bottom). b) Fits (red) to absorption spectra (black) at different spinning times and for as-prepared solution (i.e., t = 0). A novel optical signature (hatched orange) emerges from the residual of a fit consisting of the known complexes PbI_2, PbI_3^- and PbI_4^{2-}. Spectra are normalized to the central peak maximum near 3.2 eV. c) Fitting as-prepared absorption data reveals an increase of the novel signature with precursor concentration.

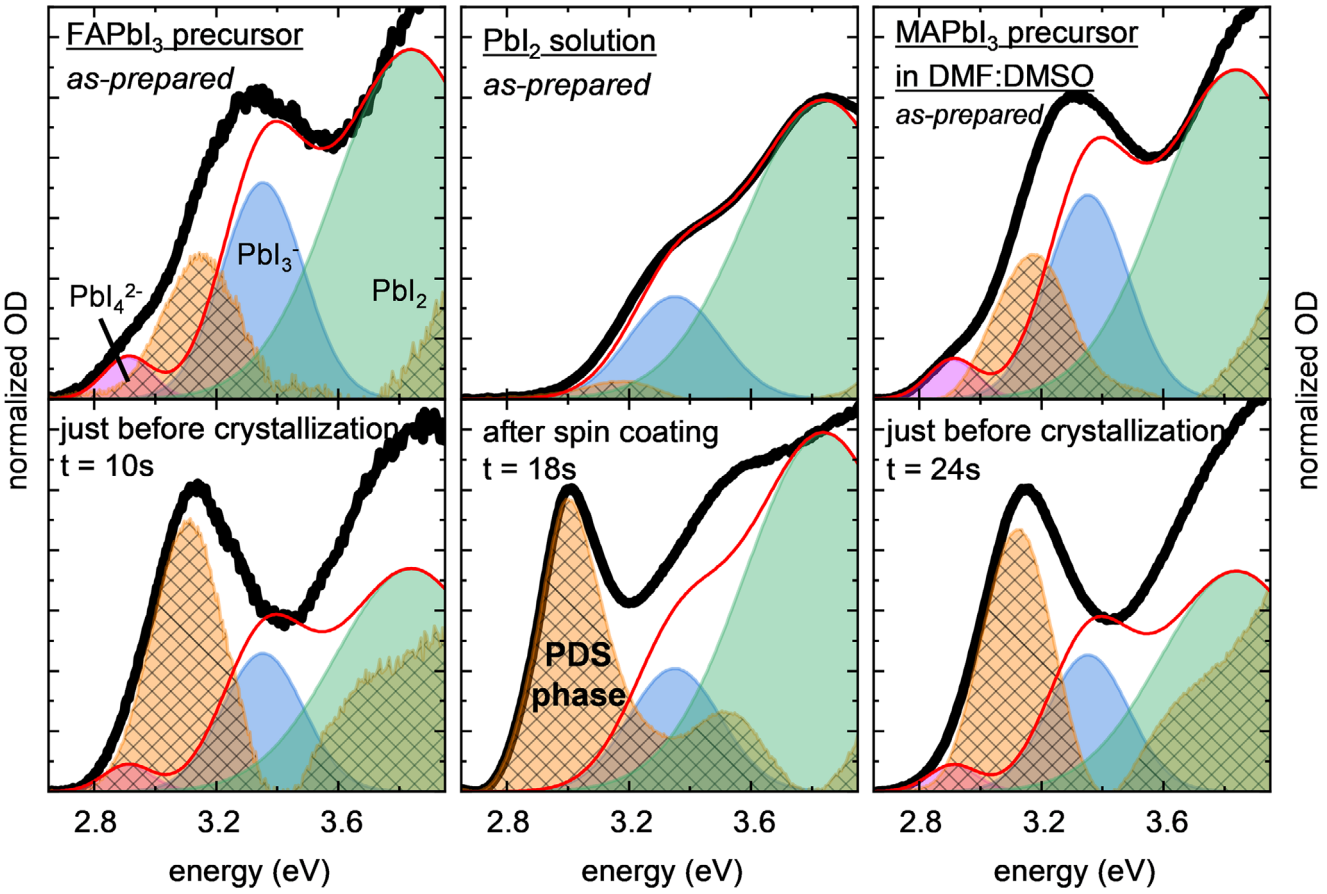

Figure 3. Fits (red) to the absorption spectra (black) of $FAPbI_3$ precursor (0.6 mol L^{-1}) in DMF, and PbI_2 (0.3 mol L^{-1}) in DMF, and $MAPbI_3$ precursor (0.6 mol L^{-1}) in a solvent mixture DMF:DMSO (12:1). Top row: spectra of as-prepared solutions. Bottom row: spectra of the solution films obtained by in situ measurements just before crystallization occurs or after spin coating. The optical signature of the PDS phase (PbI_2 solution, bottom) resembles the novel signatures in the perovskite precursor solutions. Spectra are normalized to the central peak maximum.

and would affect all iodoplumbate signatures, yet the energetic positions of PbI_4^{2-} and PbI_2 are noticeably unaffected by concentration. Figure S4 (Supporting Information) shows that fits with a shifting Gaussian near 3.2 eV give poor agreement with the measurements.

3.2. Origin of the Novel Optical Signature

Possible pathways of crystallization of hybrid perovskite have been addressed in a number of studies.[16–19] A study by Petrov et al. is particularly relevant in the context of our in situ absorption measurements in which the amount of DMF continuously reduces.[20] They developed a ternary phase diagram of MAI, PbI_2, and DMF, indicating pathways to several precipitates from precursor solutions. Their diagram suggests that depending on the initial concentration, different precipitates predominate. For the stochiometric precursor solutions we used, a PDS phase could be expected to precipitate as DMF evaporates.

We therefore explored whether the novel optical signature, indicated by the hatched orange peak in Figure 2, might be consistent with the formation of a crystalline PDS phase. Such a crystalline solvated phase has previously also been observed when spin coating a PbI_2-DMF solution.[21–23] This highly crystalline PDS phase exhibits x-ray diffraction (XRD) peaks at lower angles compared to PbI_2, indicating a larger lattice spacing due to the incorporation of DMF.[22,23] A formation of such a PDS phase has, however, not yet been associated with processes during perovskite film fabrication, nor has its optical signature been identified.

To probe this, we conducted two experiments. First, we investigated the effect of the organic cation by spin coating a formamidinium lead iodide ($FAPbI_3$) precursor dissolved in DMF and analyzing the spectra analogous to the $MAPbI_3$ precursor solution in Figure 2b. From the right panel in **Figure 3**, we see that there are no significant differences between the compositions of the $MAPbI_3$ and $FAPbI_3$ spectra, implying a negligible influence of the organic cation on the formation of the novel optical signature (see Figure S5c, Supporting Information). Second, we spin coat a solution of PbI_2 in DMF and analyze the resulting spectra as before (Figure 3, center panel). Remarkably, omitting the organic cation entirely has only a minor effect on the spectral evolution. The spectral shape still results from a superposition of the absorption features attributed to iodoplumbate complexes and the novel optical signature, with the latter increasing in the course of spin coating as the solution concentration increases.

Moreover, the spectral evolution happens on approximately the same time scale as in the $MAPbI_3$ and $FAPbI_3$ precursor solutions (see Figure S5a, Supporting Information). The differences between the spectra obtained without and with organic cation are mainly a lower fraction of PbI_4^{2-} and PbI_3^-, straightforwardly accounted for by the lower iodine concentration, and a lower final energetic position of the novel feature's peak at 3.0 eV.

The formation of a crystalline PDS phase upon spin coating PbI_2 in DMF has been identified previously by XRD and GIWAXS.[21–23] We therefore associate the residue in the fits to the data for the PbI_2 solution in Figure 3 (center panel), i.e., the hatched orange area obtained when subtracting the signatures of iodoplumbate complexes from the overall absorption, with the PDS phase. For clarification, here with PDS we exclusively refer to the sole PbI_2-DMF solvated phase, since sometimes PDS is also used for intermediate perovskite phases such as $(MA)_2Pb_3I_8(DMF)_2$.[16] In fact, we take the formation of the novel absorption peak in the PbI_2 solution, where MAI is trivially absent, as a first indication that the novel optical feature may not be associated with intermediate phases such as $(MA)_2Pb_3I_8(DMF)_2$.

When we thermally anneal the film obtained from spin coating the PbI_2 solution at 100 °C for 10 min, we observe the formation of an absorption edge at ≈2.4 eV, indicating the formation of crystalline PbI_2 (see Figure S6, Supporting Information).[24] This is consistent with the transformation of a PDS phase into crystalline PbI_2 upon annealing observed by XRD measurements and further supports our assignment.[22] In passing, we note that we observed the absorption edge at 2.4 eV to also appear without annealing when just allowing the film to dry over time.

From the similar evolution in the optical signatures during spin coating of $MAPbI_3$ or $FAPbI_3$ precursors, it is straightforward to identify the hatched orange peak around 3.2 eV in the analysis of the respective precursor solution spectra with absorption from the same PDS phase. We speculate that the rising feature above 3.7 eV might also be associated with the PDS phase, either as absorption, or perhaps as light scattering from the PDS phase.

Since perovskites are frequently prepared not from a DMF solution but from a DMF:DMSO mixture, we investigated if the signature of the PDS phase also forms in a $MAPbI_3$-DMF:DMSO precursor solution (Figure 3). Fitting the spectra with the same restrictions as before, we find the spectra for the initial solution as well as "just before crystallization" to be very similar to the spectra without DMSO. The time scale of the evolution is, however, decelerated roughly by a factor of 2 compared to pure DMF as solvent (see Figure S5b, Supporting Information).

We finally comment on the energetic shifts in the optical signature of this PDS-related peak. In the perovskite precursor data just before perovskite formation, this peak occurs at 3.15 eV, in contrast to the value of 3.0 eV in the PbI_2-DMF solution. We suggest this indicates a quantum confinement effect in the PDS structure in precursor solutions, with 3.0 eV being the energy of the absorption in the bulk PDS phase. In fact, during spin coating of PbI_2 in DMF (see Figure S5a, Supporting Information) this peak red shifts after 7 s, indicating the growth of PDS structures when no organic cation is present. Analogously, during spin coating of the precursor solution, we observe a small red shift in the PDS signal of ≈0.03 eV, which we similarly attribute to a growth of the PDS phase in the course of spin coating.

3.3. The Kinetics of PDS Phase Formation

So far, we have assigned the novel optical feature to the formation of a PDS phase, and we could observe that its intensity seems to increase with the concentration of the solution. To address this aspect in a more quantitative way, we analyzed the in situ absorption data. From a sinusoidal pattern due to thin film white light interference in the absorption at 1.6–2.3 eV, we can extract the thickness of the perovskite solution layer during spin coating (see Figure S7, Supporting Information). A comprehensive description of this method is provided by Biberger et al.[25] **Figure 4a** shows the evolution of the solution layer's thickness during spin coating of precursor solutions for different initial concentrations (c_0). The interference pattern allows to determine the thickness of the solution layer until rapid crystallization occurs after ≈10–15 s of spinning time, depending on c_0. The time of crystallization is determined by the broad overall increase of the OD (see Figure 2a), and hence the plots in Figure 4 end when the film crystallizes.

We observe several features. Generally, the higher the initial concentration of the precursor solution, the longer it takes for crystallization to occur, as evidenced by the later termination of the curves in Figure 4 (see Figure S8, Supporting Information). All measurements show a fast reduction in thickness at the beginning and a slower reduction at later times. Furthermore, the general trend is that the higher the initial concentration, the thicker the solution layer at all times.

In order to gain a deeper insight into the kinetics that govern the solution layer thinning during spin coating, we model the process as hydrodynamic-evaporative thinning. This assumes that there are two effects that determine the film thickness evolution: hydrodynamic thinning (h_{hydro}) and evaporative thinning (h_{evap}).[26,27] The hydrodynamic thinning is due to the spinning of the substrate and therefore material being thrown off. It can be described by the following equation:[28]

$$h_{hydro}(t) = h_0\left(1 + \frac{4\omega^2 h_0^2 (t - t')}{3\,\nu_{kin}}\right)^{-1/2} \quad (1)$$

h_0 is the solution layer thickness before spin coating, ω is the rotational velocity of the spin coater, ν_{kin} is the kinematic viscosity of the solution, and t is the time after starting the spin coater with an instant ramp-up in velocity. To account for the finite ramp-up time of our spin coater, we shift the model by $t' = 0.5$ s compared to the time $t = 0.0$ s where the spin coater starts accelerating. To describe the evaporative thinning, we consider that the evaporation of solvent is mainly determined by the surface area of the liquid. This holds for solutions with a negligible amount of dissolved material compared to solvent molecules, which is the case in our experiments until shortly before crystallization. Due to the large substrate area (4 cm^2), this surface stays approximately constant during the solution layer thinning. Therefore, we can assume a constant rate of evaporation E:[26,27]

$$h_{evap}(t) = -Et \quad (2)$$

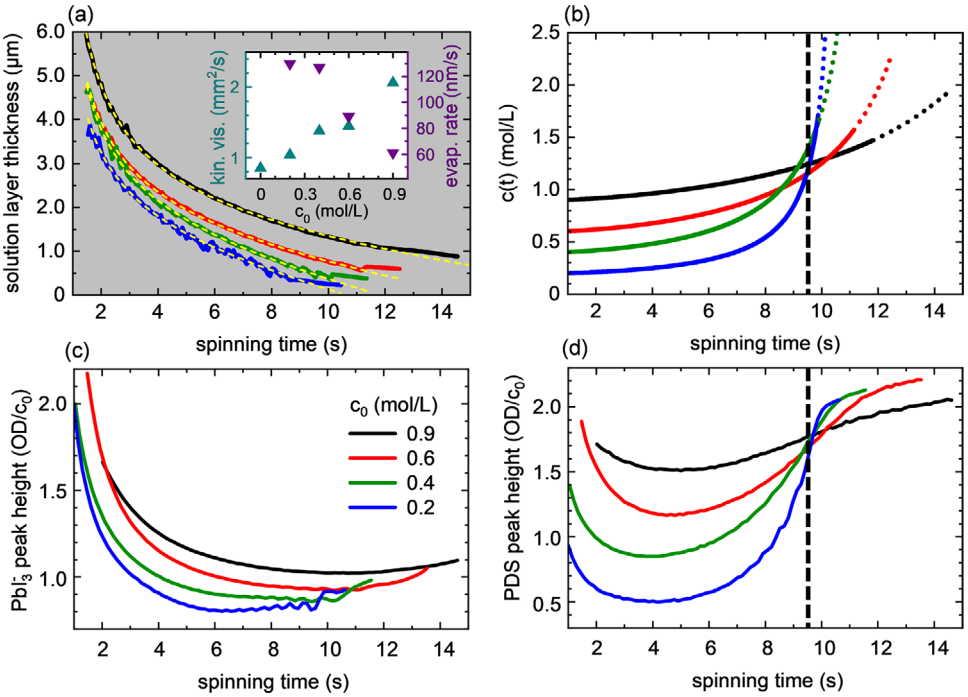

Figure 4. Analysis of in situ measurements of $MAPbI_3$ precursor in DMF. a) Thickness of the perovskite solution layer during spin coating. The kinematic viscosity (cyan) and evaporation rate (purple) are obtained from a fit (yellow) to the solution layer thickness (exception: literature value for $c_0 = 0$).[29] b) Estimated concentration evolution c(t) of the perovskite precursor solution during spin coating, according to Equation (4). c,d): Height evolutions of the spectral signatures of PbI_3^- and the PDS phase, obtained from fits to in situ measurements depicted in Figure 2. These evolutions resemble vaguely the film thickness and the concentration evolution. c_0 denotes the perovskite precursor concentration in the beginning of spin coating. The plots end when the film crystallizes. Dashed vertical lines in (b) and (d) highlight the time of intersection at 9.5 s.

Combining Equation (1) and Equation (2) yields the solution layer height model:

$$h_{\text{model}}(t) = h_{\text{hydro}}(t) + h_{\text{evap}}(t) \tag{3}$$

The initial thickness h_0 has only a minor influence on the evolution of the solvent layer thickness. We approximate h_0 as 1 mm as an estimate for the height of the droplet on the substrate before spin coating. The rotational velocity ω is 2 000 rpm, whereas the parameters ν_{kin} and E remain as fitting parameters. The yellow dotted lines in Figure 4a illustrate the best fit of Equation (3) to the data. The fit agrees with the data very well and only deviates slightly 1–2 s before crystallization occurs. As detailed below, the evaporation rate can reduce with increasing concentration. We therefore consider that 1–2 s before crystallization, the concentration has increased to a level where Equation (2) no longer applies.

The obtained fitting parameters are depicted in the inset in Figure 4a. With increasing c_0, we find an increase in kinematic viscosity and a decrease of the evaporation rate. The increase in viscosity with increasing concentration is intuitive due to an increased amount of dissolved material. Furthermore, the fitted viscosity values seem plausible when comparing them to the kinematic viscosity of DMF (0.85 $mm^2\ s^{-1}$)[29] since we expect a higher viscosity when DMF contains dissolved material. We stress that the viscosity values obtained are only valid in the hydrodynamic regime when the concentration has not changed substantially from its initial value c_0 (see S9a, Supporting Information). The fitting parameters also show a decrease in evaporation rate with increasing concentration. We explain this by the high coordinating ability of the lead complexes: solvent molecules tend to adhere to the lead, rather than to evaporate from the solution layer. This effect is greater in more concentrated solutions. The limitations of the model and the extent of the two regimes (hydrodynamic and evaporative) are further discussed in S9a (Supporting Information).

By separating the solution layer thickness evolution into a hydrodynamic and an evaporative part in our model (transition at ≈1.3 µm film thickness; see S9a, Supporting Information), we are not only able to obtain viscosities and evaporation rates, but also can estimate the evolution of the concentration during spin coating. Throw-off of material (i.e., h_{hydro}) affects the solvent as well as the solvated material in the same way. Therefore, the amount of solvated material $M(t)$ is proportional to h_{hydro}. On the other hand, the volume of solution $V(t)$ is proportional to the solution layer thickness (i.e., h_{model}). Thus, the concentration of the solution during spin coating $c(t)$ can be expressed in the following way (see S10, Supporting Information for details):

$$c(t) = \frac{M(t)}{V(t)} = \frac{c_0}{1 + \frac{h_{\text{evap}}(t)}{h_{\text{hydro}}(t)}} \tag{4}$$

Figure 4b shows the evolution of the concentration according to Equation (4), based on the fit to Figure 4a. The concentration $c(t)$ for each sample starts from its respective c_0. However,

eventually the samples with lower c_0 exceed the concentration of the samples with initially higher c_0. The dotted sections in the concentration evolution (Figure 4b) are extrapolations and highlight when the model to the film thickness evolution (Figure 4a) deviates from the measured data. Despite this, the modeled concentration evolution is consistent with previous studies identifying the solubility of $MAPbI_3$ in DMF just below 2 mol L^{-1} at room temperature.[30] S9b discusses Figure 4b in more detail.

To determine the concentration dependent formation of iodoplumbates and the PDS phase, we analyzed the in situ absorption data of $MAPbI_3$ precursors in DMF as follows. For every time frame, we fitted the absorption spectra with the model described above (see supporting video files, Supporting Information). Figure 4c shows the evolution of the absorption intensity of the PbI_3^- peak, normalized to its respective c_0. We find that the PbI_3^- peak height decreases in the beginning of spin coating and plateaus after a certain time. This can be explained simply by material throw-off. Furthermore, the transition into the plateau region roughly coincides with the transition from the hydrodynamic into the evaporative regime (c.f. S9a and S9c, Supporting Information).

The evolution of the PDS peak height, normalized to initial concentration, (Figure 4d) exhibits a more intricate dynamic. At first, the PDS phase decreases, similar to the PbI_3^- complexes. However, after ≈6 s, the PDS phase increases at different rates depending on the initial concentration of the precursor solution. Essentially, the lower the initial concentration c_0, the faster the increase after ≈6 s.

When comparing the evolution of the concentration (Figure 4b) with the evolution of the PDS phase (Figure 4d), similarities in the dynamic become apparent. Especially after 6 s, we note that the evolution of the PDS peak height qualitatively matches the concentration evolution. Despite obvious differences in the PDS phase and concentration evolution until 4 s and shortly before crystallization, the similar time evolution suggests that the evolution of the PDS phase is mainly concentration driven (c.f. S9d, Supporting Information).

The plots of the solution layer thickness in Figure 4a end when the absorption increased strongly over the entire spectral range and saturated the detector. We took this to indicate the formation of a strongly absorbing or scattering crystalline species, i.e., either the final perovskite $MAPbI_3$ or an intermediate perovskite phase such as $(MA)_2Pb_3I_8(DMF)_2$. It is intriguing that the time at which this crystallization step occurs increases with initial concentration. This can be rationalized from our insights into the evolution of the solution concentration. In the classical thermodynamic view, crystallization occurs in a supersaturated solution, i.e., when the concentration of the solution exceeds its equilibrium solubility. Since we observe that the precursor solution with a lower initial concentration crystallizes earlier (see end of plots in Figure 4 or Figure S8, Supporting Information)), supersaturation therefore also occurs earlier for initially lower concentrated solutions. This may appear counterintuitive because one could argue that lower concentrated solutions need to evaporate more solvent before reaching supersaturation. However, Figure 4b shows, that mainly the late increase in concentration after 6 s determines which solution reaches supersaturation first. In fact, lower concentrated solutions reach supersaturation earlier due to the concentration dependent evaporation and viscosity, and thereby affecting the spin coating hydrodynamics.

4. Discussion

Our UV absorption measurements, both as-prepared and in situ, give new insights into the lead iodide perovskite precursor solutions at concentrations suitable for film fabrication. Notably, fits to the absorption data reveal the emergence of a new feature that we attributed to a PbI_2-DMF-solvated (PDS) phase, independently of the organic cation (MA^+ or FA^+) (Figures 2,3). We observe that this PDS phase forms in the precursor solution with increasing concentration until the perovskite formation sets in. Hence, the PDS phase seems to be a predecessor of crystalline perovskite phases.

The earlier precipitation of MA^+-free PbI_2-like phases is also consistent with the lower solubility of PbI_2, compared to MA^+. In fact, Yan et al. describe a soft coordination framework consisting of iodine and lead that appears in solution before the formation of a perovskite phase.[8] In situ grazing incidence wide-angle x-ray scattering (GIWAXS) measurements show no high-order structures prior to the formation of the perovskite phases but rather signatures of a sol-gel phase.[15,23,31,32] Such a broad sol-gel-like signal in GIWAXS measurements would be consistent with the presence of individual, small structures in a suspension. In particular, they need to be small enough that no significant long-range order can be detected. Hence, we propose that the PDS phase in the perovskite precursor solution appears only as very small structures. This limitation on the structure size is further supported by observed peak shifts (during formation as well as when comparing PbI_2-solution with precursor signal), which we attributed to quantum confinement effects (Figure 3). It is also supported by the observations of Hu et al.[33] They observe PbI_6^{4-} octahedral cage nanoparticles in precursor solutions. Molecular dynamics simulations show that these octahedral complexes form PbI_2-like amorphous clusters by sharing edges with neighboring octahedra.[34,35] Further research needs to clarify whether the PDS phase observed here is identical to the crystalline, nanometer-scale colloids that have been observed in DMF-based $MAPbI_3$ precursor solution.[8,10,11] Importantly, our analysis enabled us to identify the optical signatures of a perovskite predecessor that we attribute to a PDS phase.

Despite the evidence brought forward so far, it is prudent to consider alternative origins for the novel absorption feature. Since our analysis is based on the optical spectra, we would not be able to distinguish between compounds with identical absorption. This is worth mentioning, in particular as the absorption energies of iodoplumbate-containing compounds are mostly determined by the metal-to-halide charge transfer. One possible, often considered intermediate in the crystallization process is $(MA)_2Pb_3I_8(DMF)_2$ solvated phase. We are not aware of its absorption spectrum being known and hence cannot exclude it being identical to PDS, though it seems unlikely that the inclusion of MA in the structure would have no influence at all on the absorption. Moreover, the formation of $(MA)_2Pb_3I_8(DMF)_2$ solvated phase would be at variance with the studies and the phase diagram by Petrov et al.[20] Another alternative possible origin could be the formation of polynuclear iodoplumbate complexes (i.e., complexes with more than one Pb atom). The delocalization of

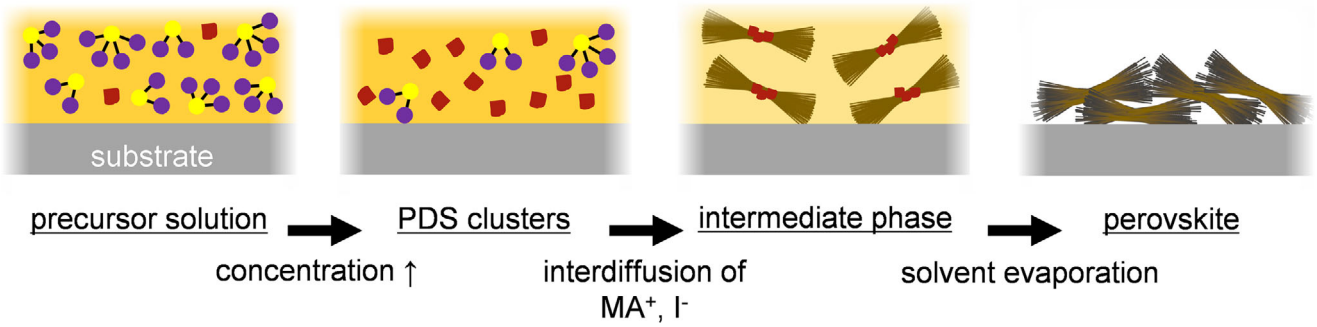

Figure 5. Mechanistic picture of the one-step spin coating process of $MAPbI_3$ precursor in DMF. We propose that PDS clusters in the precursor solution act as nucleation seeds for subsequent perovskite phases. In the end, the needle-like perovskite morphology is predetermined by the solvated intermediate phase.

the electronic system upon forming dimers and trimers leads to an energetic shift of the PbI_3^- signature.[14,36] However, also their absorption features are not unambiguously clear, and energies based on DFT calculations attributed to these polynuclear complexes are not fully consistent with the observed evolution in the band centered around 3.2 eV.[14] Given the limitations of DFT in predicting absolute energies, further work should address whether polynuclear iodoplumbate complexes can indeed definitely be ruled out.

Having associated the novel absorption feature with the formation of a PDS phase we were able to compare the growth of the PDS fraction in the solution layer to the evolution of the solutions' concentration as determined by Equation (3). The strong temporal correlation suggested that the formation of PDS phase is concentration driven. We found that as concentration increases during spin-coating, PDS formation is replaced by the formation of crystalline perovskite or intermediate perovskite. This step occurs later for higher initial concentrations. This time difference has previously been attributed to the formation of large colloids (0.1–1 μm) in the precursor solution.[37] We have instead interpreted the data in the framework of classical nucleation theory and attributed the earlier perovskite crystallization to the faster increase in concentration in the initially less concentrated solution.

The bend in the curves of Figure 4d after ≈10 s also tells us that growth of the PDS fraction reduces strongly and approaches saturation as the perovskite-based crystallites begin to form. Classical nucleation theory alone cannot account for this. One possible mechanism is the transformation of PDS into a perovskite-based phase. Cao et al. show that PDS, i.e., the PDS phase, can transform into crystalline $MAPbI_3$ through a molecular exchange of the DMF in the PDS phase with MA^+ and I^- ions.[22] During spin coating, however, solvated intermediate perovskite phases typically form prior to unsolvated $MAPbI_3$.[38,39] Therefore, we tentatively suggest that PDS clusters primarily convert into $(MA)_2Pb_3I_8(DMF)_2$ via interdiffusion of MAI, before finally changing over to $MAPbI_3$, consistent with simulations from Ahlawat et al.[35]

Based on the results presented in this work, in combination with those of other research groups,[7,8,15,22,32,39,40] we propose a mechanism (**Figure 5**) for the evolution of the precursor chemistry and the resulting film formation in the one-step spin coating process that includes the appearance of a temporary PDS phase. At first, iodoplumbate complexes as well as few small PDS clusters are present in the as-prepared lead iodide perovskite precursor solution (see Figure 2).[6,8] During spin coating and with increasing concentration, the number of PDS clusters increases. This process is mainly concentration driven. Eventually, at larger concentrations (roughly in the range exceeding 1.7 mol L^{-1}, see Figure 4b), the organic cation begins to diffuse into the PDS clusters. This prevents further PDS formation and instead enables the formation of primarily intermediate perovskite. In this way, the original PDS clusters become nucleation seeds for the further growth of the intermediate perovskites, which occurs in an anisotropic way to result in a needle-like structure.[19] Finally, the complete solvent removal (typically accelerated via heat treatment) results in the solvent-free perovskite phase. The final needle-like structure illustrated in Figure 5 is predetermined by the structure of the intermediate phase.[19]

5. Conclusion

In summary, we investigated the precursor chemistry and its evolution in different concentrated solutions both before (as-prepared) and during spin coating (in situ). We identify absorption features from iodoplumbate complexes as well as from PDS clusters. Quantum confinement effects suggest that this PDS phase appears only as small structures during processing of lead iodide perovskites, rather than as bulk crystalline structures with long-range order. Based on our analysis of the solutions' concentration and the observed absorption features, we infer that the PDS phase evolves into intermediate perovskite and hence plays a central role in the perovskite crystallization process.

Therefore, PDS phase engineering presents itself as a promising way to refine perovskite crystallization and optimize film morphology without additional post treatments. In particular, we anticipate that PDS crystallites are not only involved in the one-step spin coating process, but also in other coating processes and fabrication procedures. Hence, two-step procedures, gas quenching or antisolvent methods should consider the PDS phase in their protocol for film fabrication. For instance, the amount of PDS clusters in the solution may also be useful for determining when antisolvent should be added in an automated way ("reac-

tive concept").[25] Additive engineering of the precursor solution would be a further promising approach to modify the PDS phase.

Our study elucidates the critical role of PDS clusters in the formation of lead iodide perovskites, offering a better understanding of the precursor chemistry and crystallization dynamics. An optical signature reveals the amount of this PDS phase (even during fabrication) and can be used to optimize the film formation, for instance by controlling the amount of nucleation sites during perovskite crystallization. Future research should further explore film fabrication methods and their impact on the PDS phase, subsequent perovskite phases, and film morphology. The integration of these insights into existing fabrication techniques holds promise for innovative approaches in perovskite solar cell production (Videos 1–4, Supporting Information).

Supporting Information

Supporting Information is available from the Wiley Online Library or from the author.

Acknowledgements

The authors thank Fabian Panzer and Konstantin Schötz for initiating this work, and Helen Grüninger for fruitful discussions. FE and EMH thank the Deutsche Forschungsgemeinschaft (DFG Research Unit FOR 5387 POPULAR, Project No. 461909888) for their support. EMH and AK acknowledge DFG PA 3373/7-1 for funding.

Conflict of Interest

The authors declare no conflict of interest.

Author Contributions

MS and SB planned the experiments. MS modified the in situ setup and conducted all in situ measurements and their analysis. FE under the supervision of EMH conducted the as-prepared UV–vis absorption spectroscopy measurements with the TFFS method. MS developed the precursor states fitting, the model for the film thickness and concentration evolution and modeled all absorption spectra. MS, SB, and AK discussed the results and outlined the manuscript. MS with help from SB wrote the first version of the manuscript. AK edited the manuscript. All authors critically read the manuscript and commented on the manuscript. AK supervised the project.

Data Availability Statement

The data that support the findings of this study are available from the corresponding author upon reasonable request.

Keywords

iodoplumbate complexes, methylammonium lead iodide, optical spectroscopy, precursor chemistry, precursor properties, sol-gel, solution engineering

Received: January 21, 2025
Revised: March 15, 2025
Published online: April 21, 2025

[1] *Best Research-Cell Efficiency Chart*, https://www.nrel.gov/pv/cell-efficiency.html (accessed: April 2025).
[2] W. Nie, H. Tsai, R. Asadpour, J.-C. Blancon, A. J. Neukirch, G. Gupta, J. J. Crochet, M. Chhowalla, S. Tretiak, M. A. Alam, H.-L. Wang, A. D. Mohite, *Science* **2015**, *347*, 522.
[3] M. Saliba, J.-P. Correa-Baena, C. M. Wolff, M. Stolterfoht, N. Phung, S. Albrecht, D. Neher, A. Abate, *Chem. Mater.* **2018**, *30*, 4193.
[4] O. Horváth, I. Mikó, *J. Photochem. Photobiol., A* **1998**, *114*, 95.
[5] K. G. Stamplecoskie, J. S. Manser, P. V. Kamat, *Energy Environ. Sci.* **2015**, *8*, 208.
[6] E. Radicchi, E. Mosconi, F. Elisei, F. Nunzi, F. De Angelis, *ACS Appl. Energy Mater.* **2019**, *2*, 3400.
[7] J. C., jr. Hamill, J. Schwartz, Y.-L. Loo, *ACS Energy Lett.* **2018**, *3*, 92.
[8] K. Yan, M. Long, T. Zhang, Z. Wei, H. Chen, S. Yang, J. Xu, *J. Am. Chem. Soc.* **2015**, *137*, 4460.
[9] J. Kim, B. Park, J. Baek, J. S. Yun, H.-W. Kwon, J. Seidel, H. Min, S. Coelho, S. Lim, S. Huang, K. Gaus, M. A. Green, T. J. Shin, A. W. Y. Ho-baillie, M. G. Kim, S. I. Seok, *J. Am. Chem. Soc.* **2020**, *142*, 6251.
[10] M. E. O'Kane, J. A. Smith, R. C. Kilbride, E. L. K. Spooner, C. P. Duif, T. E. Catley, A. L. Washington, S. M. King, S. R. Parnell, A. J. Parnell, *Chem. Mater.* **2022**, *34*, 7232.
[11] N. S. Dutta, N. K. Noel, C. B. Arnold, *J. Phys. Chem. Lett.* **2020**, *11*, 5980.
[12] F. Eller, E. M. Herzig, *J. Phys. Chem. A* **2024**, *128*, 9682.
[13] M. Buchhorn, S. Wedler, F. Panzer, *J. Phys. Chem. A* **2018**, *122*, 9115.
[14] A. M. Valencia, O. Shargaieva, R. Schier, E. Unger, C. Cocchi, *J. Phys. Chem. Lett.* **2021**, *12*, 2299.
[15] R. Munir, A. D. Sheikh, M. Abdelsamie, H. Hu, L. Yu, K. Zhao, T. Kim, O. E. Tall, R. Li, D.-M. Smilgies, A. Amassian, *Adv. Mater.* **2017**, *29*, 1604113.
[16] L. Ke, S. Luo, X. Ren, Y. Yuan, *J. Phys. D: Appl. Phys.* **2021**, *54*, 163001.
[17] Z. Wu, S. Sang, J. Zheng, Q. Gao, B. Huang, F. Li, K. Sun, S. Chen, *Angew. Chem., Int. Ed.* **2024**, *63*, 202319170.
[18] I. Hwang, *J. Phys. Chem. C* **2023**, *127*, 24011.
[19] A. A. Petrov, I. P. Sokolova, N. A. Belich, G. S. Peters, P. V. Dorovatovskii, Y. V. Zubavichus, V. N. Khrustalev, A. V. Petrov, M. Grätzel, E. A. Goodilin, A. B. Tarasov, *J. Phys. Chem. C* **2017**, *121*, 20739.
[20] A. A. Petrov, A. A. Ordinartsev, K. A. Lyssenko, E. A. Goodilin, A. B. Tarasov, *J. Phys. Chem. C* **2022**, *126*, 169.
[21] H. Zheng, W. Wang, S. Yang, Y. Liu, J. Sun, *RSC Adv.* **2016**, *6*, 1611.
[22] X. B. Cao, Y. H. Li, F. Fang, X. Cui, Y. W. Yao, J. Q. Wei, *RSC Adv.* **2016**, *6*, 70925.
[23] D. Barrit, P. Cheng, M.-C. Tang, K. Wang, H. Dang, D.-M. Smilgies, S. (Frank) Liu, T. D. Anthopoulos, K. Zhao, A. Amassian, *Adv. Funct. Mater.* **2019**, *29*, 1807544.
[24] D.-Y. Lin, B.-C. Guo, Z.-Y. Dai, C.-F. Lin, H.-P. Hsu, *Crystals* **2019**, *9*, 589.
[25] S. Biberger, M. Spies, K. Schötz, F.-J. Kahle, N. Leupold, R. Moos, H. Grüninger, A. Köhler, F. Panzer, *J. Mater. Chem. C* **2024**, *12*, 6415.
[26] J. Danglad-Flores, S. Eickelmann, H. Riegler, *Eng. Rep.* **2021**, *3*, 12390.
[27] S. Karpitschka, C. M. Weber, H. Riegler, *Chem. Eng. Sci.* **2015**, *129*, 243.
[28] N. Sahu, B. Parija, S. Panigrahi, *Indian J. Phys.* **2009**, *83*, 493.
[29] P. S. Nikam, S. J. Kharat, *J. Chem. Eng. Data* **2005**, *50*, 455.
[30] A. A. Petrov, A. A. Ordinartsev, S. A. Fateev, E. A. Goodilin, A. B. Tarasov, *Molecules* **2021**, *26*, 7541.
[31] Y. Zhong, R. Munir, J. Li, M.-C. Tang, M. R. Niazi, D.-M. Smilgies, K. Zhao, A. Amassian, *ACS Energy Lett.* **2018**, *3*, 1078.
[32] J. Li, R. Munir, Y. Fan, T. Niu, Y. Liu, Y. Zhong, Z. Yang, Y. Tian, B. Liu, J. Sun, D.-M. Smilgies, S. Thoroddsen, A. Amassian, K. Zhao, S. (Frank) Liu, *Joule* **2018**, *2*, 1313.

[33] Q. Hu, L. Zhao, J. Wu, K. Gao, D. Luo, Y. Jiang, Z. Zhang, C. Zhu, E. Schaible, A. Hexemer, C. Wang, Y. Liu, W. Zhang, M. Grätzel, F. Liu, T. P. Russell, R. Zhu, Q. Gong, *Nat. Commun.* **2017**, *8*, 15688.
[34] B. Li, Q. Dai, S. Yun, J. Tian, *J. Mater. Chem. A* **2021**, *9*, 6732.
[35] P. Ahlawat, A. Hinderhofer, E. A. Alharbi, H. Lu, A. Ummadisingu, H. Niu, M. Invernizzi, S. M. Zakeeruddin, M. I. Dar, F. Schreiber, A. Hagfeldt, M. Grätzel, U. Rothlisberger, M. Parrinello, *Sci. Adv.* **2021**, *7*, abe3326.
[36] J. Jiang, J. M. Vicent-Luna, S. Tao, *J. Energy Chem.* **2022**, *68*, 393.
[37] C. Rehermann, V. Schröder, M. Flatken, F. Ünlü, O. Shargaieva, A. Hoell, A. Merdasa, F. Mathies, S. Mathur, E. L. Unger, *RSC Adv.* **2022**, *12*, 32765.
[38] W. Xiang, J. Zhang, S. (Frank) Liu, S. Albrecht, A. Hagfeldt, Z. Wang, *Joule* **2022**, *6*, 315.
[39] K. Schötz, C. Greve, A. Langen, H. Gorter, I. Dogan, Y. Galagan, A. J. J. M. van Breemen, G. H. Gelinck, E. M. Herzig, F. Panzer, *Adv. Opt. Mater.* **2021**, *9*, 2101161.
[40] M. A. Reus, L. K. Reb, A. F. Weinzierl, C. L. Weindl, R. Guo, T. Xiao, M. Schwartzkopf, A. Chumakov, S. V. Roth, P. Müller-Buschbaum, *Adv. Opt. Mater.* **2022**, *10*, 2102722.

